Research Article

Fazal Wahed, Ata-ur-Rahman, S. Neelam Naeem, R. A. Alharbey, Maryam Al Huwayz, Lamiaa S. El-Sherif, and Samir A. El-Tantawy*

Modulational instability and associated ion-acoustic modulated envelope solitons in a quantum plasma having ion beams

https://doi.org/10.1515/phys-2025-0180
received March 08, 2025; accepted May 17, 2025

Abstract: This work employs the one-dimensional quantum hydrodynamic model to investigate the nonlinear propagation of modulated ion-acoustic waves (IAWs) in unmagnetized quantum plasma with ion beams. A reductive perturbation technique (RPT) is carried out to reduce the set of fluid equations to a cubic nonlinear Schrödinger equation (NLSE), which governs the propagation of the modulational instability (MI) and its associated modulated structures (envelope solitons). It is demonstrated that plasma configurational parameters, such as ion beam density, quantum diffraction parameter, and ion beam temperature, significantly affect MI and the related nonlinear structures. We also examined the impact of these pertinent physical parameters on the critical wavenumber and the growth rates related to MI. The critical wavenumber and MI growth rate were found to decrease with growing values of quantum diffraction parameters and ion beam temperature while falling with ion beam density. Furthermore, the modulated nonlinear localized structures that appear as bright and dark envelope solitons are discussed in detail. Our results are expected to reveal the mystery of the behavior of the modulated nonlinear phenomena that may arise and propagate in such a type of quantum plasma with ion beams. Moreover, the results can be used to understand the behavior of many modulated nonlinear phenomena and then devote them to various applications.

Keywords: quantum plasma, ion beams, nonlinear Schrödinger equation, modulational instability, ion-acoustic modulated solitons

1 Introduction

Quantum plasmas have been vigorously studied over the past few decades due to their importance in ultracold plasmas [1], strong laser plasma interaction experiments [2], microelectronic devices [3], microplasmas [4], and astrophysical conditions like neutron stars, white dwarfs [5,6]. Quantum plasma consists of ions, electrons, and positrons at high number densities and small temperatures, whereas classical plasma is characterized by small particle number densities and high temperatures. The plasma particles' de Broglie wavelengths in a classical plasma are substantially less than the system's size. Nonetheless, the de Broglie thermal wavelengths of the plasma particles in quantum plasma get closer to the system's spatial scale [7,8]. In the latter case, the Heisenberg and Pauli exclusion principles govern plasma species, and quantum effects can be analyzed through the quantum Bohm potential force and quantum statistics [9]. In quantum plasmas, the charged particles' length, time, and thermal velocities differ greatly from those in traditional plasmas. Therefore, while dealing with quantum plasmas, one must appropriately modify mathematical formulations used in classical situations. The statistical and hydrodynamic behaviors of

* **Corresponding author: Samir A. El-Tantawy,** Department of Physics, Faculty of Science, Port Said University, Port Said 42521, Egypt; Department of Physics, Faculty of Science, Al-Baha University, Al-Baha, P.O. Box 1988, Saudi Arabia, e-mail: tantawy@sci.psu.edu.eg, samireltantawy@yahoo.com
Fazal Wahed: Department of Physics, Government Post Graduate College Khar, Bajaur, Pakistan; Department of Physics, Islamia College Peshawar, Peshawar 25120, Pakistan
Ata-ur-Rahman, S. Neelam Naeem: Department of Physics, Islamia College Peshawar, Peshawar 25120, Pakistan
R. A. Alharbey: Mathematics Department, Faculty of Science, King Abdulaziz University, P.O. Box 42696, Jeddah 21551, Saudi Arabia
Maryam Al Huwayz: Department of Physics, College of Science, Princess Nourah bint Abdulrahman University, P.O. Box 84428, Riyadh 11671, Saudi Arabia
Lamiaa S. El-Sherif: Department of Physics, College of Science and Humanities in Al-Kharj, Prince Sattam bin Abdulaziz University, Al-Kharj 11942, Saudi Arabia; Department of Physics, Faculty of Science, Ain Shams University, Cairo, Egypt

plasma particles at the quantum scale are described using well-known mathematical techniques such as Schrödinger–Poisson, Winger–Poisson, and Dirac–Maxwell. The behavior of plasma particles and collective phenomena including waves, nonlinear structures, and instabilities at the quantum scale, however, can be studied effectively using the quantum hydrodynamic (QHD) model [10–12]. The QHD model includes a set of fundamental equations describing the transport of momentum, energy, and charge associated with plasma particles interacting *via* self-consistent electrostatic potential. The QHD model generalizes the fluid model for plasma by incorporating the quantum correction term, or Borm potential (due to quantum tunneling effects), and the quantum statistical effect through an equation of state. The QHD model has attained significant importance compared to other quantum plasma models due to its analytical tractability and simple numerical modeling, even though it has been failed to explain kinetic effects like the Landau damping of waves [13]. Due to straightforward approach, numerical efficiency, and simplicity, the QHD model has been extensively used by researchers. For example, Haas and Garcia investigated the significance of quantum diffraction in both linear and nonlinear regimes using the QHD model [14]. Ion acoustic solitary waves (IASWs) in a quantum electron–positron–ion (e–p–i) plasma with weakly transverse disturbances were examined by Mushtaq and Khan using the QHD model [15]. Using the same model, Rajabi and Muhammadneja [16] investigated IASWs in dense quantum plasma. Futhermore, Chandra *et al.* [17] have also statistically and theoretically examined the linear and nonlinear propagation of electron plasma waves in a two-component unmagnetized dense quantum plasma with ion streaming using the QHD model.

Nonlinear wave propagation in ion beam plasma has garnered a lot of attention because of its important uses in heavy ion inertial fusion [18–20], semiconductor lasers [21–24], electron cooling of ion beams [25–29], and intense laser-produced proton beams [30–32]. The research on the latter also contributes to the fields of astrophysics and magnetospheric physics [33–37]. The presence of ion beams significantly affects nonlinear structures in plasmas [38], and the ion beam–plasma interactions process in various plasma environments has been actively studied [39,40]. For example, in an ion beam plasma system with cold ion beams and nonisothermal electrons, Abrol and Tagare derived a modified KdV equation for IASWs [41]. Gell and Roth [42] examined the effect of an ion beam on soliton motion in the ion beam–plasma system. Many authors have since examined solitary waves (SWs) in ion beam plasma, like Das and Deka [43], Misra and Adhikary [44], Huibin and Kelin [45], Zank and McKenzie [46], Karmakar and Das [47], *etc*. Recently, Kaur *et al.* [48] studied the nonlinear propagation of IASWs in an unmagnetized plasma that included two temperature electrons, a positive ion beam, and a positive warm ion fluid. Additionally, Kaur *et al.* [49] investigated dust acoustic solitary and rogue wave (RW) propagation characteristics in an unmagnetized ion beam plasma.

Due to the self-interaction of the carrier wave or intrinsic nonlinearity of the medium, amplitude modulation is frequently observed during nonlinear wave propagation in ion beam plasma or dispersive medium [50]. While investigating amplitude modulation, the multiple space and time-scale technique [51] is commonly used, which results in a Kortwege-de Vires (KdV) equation and nonlinear Schrödinger equation (NLSE). The KdV equation and all its family (*e.g.*, modified KdV, extended/Gardner KdV, Schamel-KdV equations, *etc*.) describe the dynamics of non-modulated wave packets, which are bare pulses without rapid oscillations within the packets [52–58]. In contrast, the NLSE describes the behavior of modulated wave packets so that wave group dispersion balances nonlinearities [59–61]. The NLSE has stationary envelope solutions, *i.e.*, envelope solitons. These solitons are the localized structures that take the form of localized envelope excitations, which confine, or modulate, a fast internal carrier wave oscillation in space [62]. The detailed analysis of the soliton solution of NLSE can be seen in previous studies [63–68]. Moreover, through analytical and numerical investigations, it has been discovered that modulated wavepackets are related to modulational instability (MI) [69]. MI is a significant nonlinear phenomenon that occurs during propagation of wavepackets and has been studied in many different physical contexts, including solid-state physics [70], hydrodynamics [71], plasma physics [72], and Bose–Einstein condensation [73,74]. The latter has many applications in charge transport in molecular systems [75], signal transmission lines [76], and fiber telecommunications [77]. Watanabe reported the first experimental observation of the MI of a monochromatic ion-acoustic wave (IAW) in 1977 [78]. The MI and associated envelope structures were studied by Irshad *et al.* [79] in a non-Maxwellian plasma consisting of inertialess κ-deformed Kaniadakis distributed electrons, inertial cold fluid electrons, and stationary positive ions. Wahed *et al.* [80] investigated the MI and associated low-frequency dust-acoustic waves in a degenerate Thomas-Fermi plasmas. Similarly, the MI of IASWs and associated RWs in ultracold plasmas in the presence of an ion kinematic viscosity were examined by El-Tantawy [81]. Furthermore, Kourakis and Shukla [82] investigated the MI of electron acoustic waves in space

plasmas characterized by inertialess Boltzmann-distributed hot electrons, inertial cold electrons, and static ions.

To our knowledge, there are no relevant studies in the literature on the significance of the MI and the creation of (un)stable envelope structures in the context of (un)stable electrostatic wavepacket propagation in ion-beam plasma systems. Therefore, in the presence of an ion beam, we studied the impact of various factors on the dynamics of amplitude-modulated IAWs and envelope structures in unmagnetized quantum degenerate plasma. Our findings show that plasma configurational parameters, such as ion beam temperature, diffraction parameter, and density, have a great effect on MI. These parameters can change both the associated critical values and the growth rates of MI.

The structure of the article proceeds as follows: In Section 2, we present the fundamental equations governing the dynamics of IAWs in unmagnetized quantum plasma, considering the influence of an ion beam. Section 3 is devoted to the use of reductive perturbation technique (RPT) to derive the NLSE. The MI and its growth rate are discussed in Section 4. In Section 5, we provide a comprehensive study of both bright and dark envelope solitons, including a parametric investigation of key variables such as the ion beam density ratio n_{bo}, the diffraction parameter H, and the ion beam temperature δ_b. Finally, we summarize our findings in Section 6.

2 Basic equations

An unmagnetized, collisionless quantum plasma model made up of ion beams, positive ions, and inertialess electrons is examined in this work. All species in the plasma are assumed to adhere to the Fermi–Dirac statistics, and the positive ions and positive ion beams are regarded as singly ionized. The low-frequency IAWs are sustained *via* two competing mechanisms: the mass of ion is responsible for the inertia while the restoring force is supplied by the massless electrons to keep IAWs to propagate. The IAWs' phase velocity is substantially higher than the Fermi velocity of positive ion beams and substantially lower than the electron's Fermi velocity. At zero temperature, it is assumed that the plasma particles follow the following pressure law and act like a one-dimensional Fermi gas [14]

$$P_j = \frac{M_j V_{Fj}^2}{3N_{jo}^2} \times N_j^3, \tag{1}$$

where $j = i$, b, and e stands for ions, ion beams, and electrons, respectively. The Fermi speed is $V_{Fj} = \sqrt{(2k_B T_{Fj})/M_j}$, where k_B and T_{Fj} are the Boltzmann constant and Fermi temperature. The number density and equilibrium number density are represented by N_j and N_{jo}, respectively. The electron plasma frequency is $\omega_{pe} = \sqrt{(4\pi N_o e^2)/M_e}$. The normalized one-dimensional equations governing plasma dynamics [83] are as follows:

$$\partial_x \phi - N_e \partial_x N_e + \frac{H^2}{2}\partial_x\left(\frac{1}{\sqrt{N_e}}\partial_x^2\sqrt{N_e}\right) = 0, \tag{2}$$

$$\partial_t N_i + \partial_x(N_i V_i) = 0, \tag{3}$$

$$\partial_t V_i + V_i \partial_x V_i = -\delta_i N_i \partial_x N_i + \mu \partial_x \phi, \tag{4}$$

$$\partial_t N_b + \partial_x(N_b V_b) = 0, \tag{5}$$

$$\partial_t V_b + V_b \partial_x V_b + \mu\delta_b \partial_x \phi = -\delta_b N_b \partial_x N_b, \tag{6}$$

$$\partial_x^2 \phi = \chi N_e - N_i - N_b(1-\chi). \tag{7}$$

To simplify the analysis, the normalization of the spacial (x) and temporal (t) variables is, respectively, carried out *via* $x\omega_{pi}/V_{Fi}$ and $t\omega_{pi}$. The number densities of the current model species N_j, electric potential ϕ, and speed u_j are normalized by $N_j/_{No}$, $e\varphi/(2k_B T_{Fj})$, and V_j/V_{Fe}, respectively. The ratio between the masses of positive ion and ion beams, positive ion (beam) Fermi temperature to electron Fermi temperature, and unperturbed electron number density and ion number density are, respectively, given by $\mu = m_i/m_b$ (mass ratio), $\delta_{i,b} = T_{Fi,b}/T_{Fe}$ (ion temperature ratio/ion beam temperature ratio), and $\chi = N_{eo}/N_{io}$ (electron concentration). The ratio of plasma energy $\hbar\omega_{pe}$ to Fermi energy $k_B T_{Fe}$ is equal to the dimensionless quantum parameter H, which is proportional to quantum diffraction.

The QHD model for IAWs in unmagnetized quantum plasma with ion beams is represented by Eqs. (2)–(7). The quantum correction is incorporated through the third term on the left side in Eq. (2), which arises from the quantum correlation of density variations and is referred to as the Bohm potential or quantum pressure. Other contributions to the quantum effects in this model stem from the first terms on the right sides in Eqs (4) and (6), respectively. The latter terms are incorporated through Eq. (1). The electric potential ϕ can be obtained by integrating Eq. (2) with boundary conditions $N_e = 1$ and $\phi = 0$ at $\pm\infty$ as

$$\phi = -\frac{1}{2} + \frac{N_e^2}{2} - \frac{H^2}{2}\left(\frac{1}{\sqrt{N_e}}\partial_x^2\sqrt{N_e}\right).$$

3 Perturbative analysis and derivation of NLSE

Nonlinear partial differential equations (PDEs) can be solved using various techniques, including the RPT,

Adomian decomposition technique, variational iteration technique, differential transform technique, reduced differential transform technique, and the simplest equation technique [84,85]. The RPT is particularly effective for studying nonlinear waves with small amplitudes. The RPT was established by Taniuti and Wei [51] and was first used to investigate the dynamics of electron plasma [86] and electron–cyclotron waves [87,88]. This technique has been referred to as an RPT since it reduces the behavior of the system's PDEs to the solution of nonlinear equations [89]. In the RPT, both spatial and temporal variables are rescaled, and new variables are introduced into the fundamental equations that describe long-wavelength phenomena. This method is widely used in quantum plasma because of its systematic approach, improved computational efficiency, and ability to effectively manage weak nonlinearity and dispersion. According to this technique, the smallness parameter $\varepsilon \ll 1$, which represents a weak perturbation impact, is used to expand the state variables related to random perturbations around the equilibrium states [90]. Let S be any of the system variables $(N_e, N_i, N_b, V_i, V_b, \phi)$ that represent the state of the system at position x and time t. The expansion for S around the equilibrium state $S^{(0)} = (\chi, 1, 1-\chi, 0, 0, 0)$ reads

$$S = S^{(0)} + \sum_{n=1}^{\infty} S^{(n)},$$

with

$$S^{(n)} = \sum_{l=-\infty}^{\infty} S_l^{(n)} \exp[il(kx - \omega t)].$$

All state variables satisfy the reality condition $S_{-l}^{(n)} = S_l^{(n)^*}$. According to Gardner and Morikawa's [91] suggestion, the space and time coordinates are stretched as $\xi = (x - tv_g)\varepsilon$ and $\tau = t\varepsilon^2$, where v_g will be determined later and is the group velocity of the wavepacket. The spatial and time operators then take the following form:

$$\begin{bmatrix} \partial_x \\ \partial_t \end{bmatrix} = \begin{bmatrix} \partial_x \\ \partial_t \end{bmatrix} + \varepsilon \begin{bmatrix} \partial_\xi \\ -v_g \partial_\xi \end{bmatrix} + \varepsilon^2 \begin{bmatrix} 0 \\ \partial_\tau \end{bmatrix}. \tag{8}$$

All the dependent variables $N_e, N_i, N_b, V_i, V_b, \phi$ can be expanded in terms of ε as

$$\begin{bmatrix} N_e(x,t) \\ N_i(x,t) \\ N_b(x,t) \\ V_i(x,t) \\ V_b(x,t) \\ \phi(x,t) \end{bmatrix} = \begin{bmatrix} N_{eo} \\ N_{io} \\ N_{bo} \\ 0 \\ 0 \\ 0 \end{bmatrix} + \sum_{n=1}^{\infty} \varepsilon^n \sum_{l=-\infty}^{\infty} \begin{bmatrix} N_{el}^{(n)}(\xi,\tau) \\ N_{il}^{(n)}(\xi,\tau) \\ N_{bl}^{(n)}(\xi,\tau) \\ V_{il}^{(n)}(\xi,\tau) \\ V_{bl}^{(n)}(\xi,\tau) \\ \phi_l^{(n)}(\xi,\tau) \end{bmatrix} e^{i(kx-\omega t)l}. \tag{9}$$

Substituting the above Eq. (9) into the system (2)–(7) and using Eq. (8) along with stretched coordinates, the following reduced equations in the lowest order of ε for first-order $n = 1$ and $l = 1$ are obtained:

$$\begin{cases} 4\chi\phi_1^{(1)} - N_{e1}^{(1)}(4\chi^2 + k^2H^2) = 0, \\ -\omega N_{i1}^{(1)} + k u_{i1}^{(1)} = 0, \\ -\omega V_{i1}^{(1)} + k\phi_1^{(1)} + \delta_i k N_{i1}^{(1)} = 0, \\ -\omega N_{b1}^{(1)} + k(1-\chi)V_{b1}^{(1)} = 0, \\ -\omega V_{b1}^{(1)} + \mu k\phi_1^{(1)} + \mu\delta_b k(1-\chi)N_{b1}^{(1)} = 0, \\ \chi N_{e1}^{(1)} - N_{i1}^{(1)} - (1-\chi)N_{b1}^{(1)} + k^2\phi_1^{(1)} = 0. \end{cases} \tag{10}$$

In terms of $\phi_1^{(1)}$, the first-order quantities are given by

$$\begin{cases} N_{e1}^{(1)} = \left(\dfrac{4\chi}{4\chi^2 + k^2H^2}\right)\phi_1^{(1)}, \\ N_{i1}^{(1)} = \left(\dfrac{-k^2}{k^2\delta_i - \omega^2}\right)\phi_1^{(1)}, \\ V_{i1}^{(1)} = \left(\dfrac{-k\omega}{k^2\delta_i - \omega^2}\right)\phi_1^{(1)}, \\ N_{b1}^{(1)} = \left(\dfrac{k^2(1-\chi)\mu}{\omega^2 - k^2\mu\delta_b(1-\chi)^2}\right)\phi_1^{(1)}, \\ V_{b1}^{(1)} = \left(\dfrac{-k\omega\mu}{-\omega^2 + k^2\mu\delta_b - 2k^2\chi\mu\delta_b + k^2\chi^2\mu\delta_b}\right)\phi_1^{(1)}. \end{cases} \tag{11}$$

The following dispersion relation is the result of the above first-order quantities:

$$\begin{aligned} \omega^2 = {} & \frac{1}{2H^2k^4 + 8(1+k^2)\chi^2}(k^2(H^2k^2 + 4\chi^2) \\ & \times [1 + (\chi-1)^2\mu] \\ & + [k^4((H^2k^2 + 4\chi^2)^2(1 + (\chi-1)^2\mu)^2 \\ & + (H^2k^4 + 4(1+k^2)\chi^2)(2(H^2k^2 + 4\chi^2)(-1 \\ & + (-1+\chi)^2\mu) + (H^2k^4 \\ & + 4(1+k^2)\chi^2)((\chi-1)^2\mu\delta_b - \delta_i)) \\ & \times ((\chi-1)^2\mu\delta_b - \delta_i))]^{\frac{1}{2}} + k^2(H^2k^4 \\ & + 4(1+k^2)\chi^2)((\chi-1)^2\mu\delta_b + \delta_i)). \end{aligned} \tag{12}$$

In the presence of ion beams, the dispersion relation for the IAWs in an unmagnetized quantum (degenerate) plasma is represented by Eq. (12). It is noted that the dispersion relation depends on ion beam density n_{bo}, quantum parameter H, and ion beam temperature δ_b. Figure 1(a) illustrates that ω increases as the values of k increase for a fixed value of n_{bo}. It is also noted that when n_{bo} is increased, ω is shifted toward larger values. Figure 1(b) and (c) illustrates that for smaller values of k, the frequency ω has the same value for given values of H and δ_b; however, for larger values of k, the frequency ω shifts toward larger values for increasing values of H and δ_b.

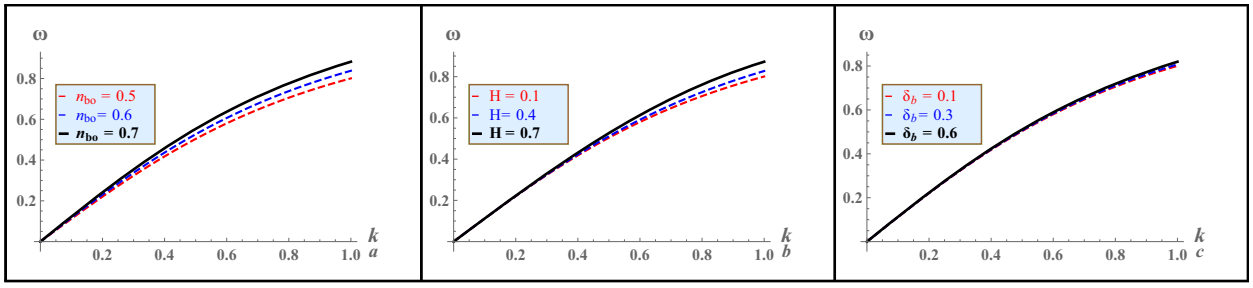

Figure 1: The wave frequency ω is analyzed against (a) ion beam density n_{bo} for fixed values of $H = 0.1$ and $\delta_b = 0.1$, (b) quantum diffraction parameter H for fixed values of $n_{bo} = 0.5$ and $\delta_b = 0.1$, and (c) ion beam temperature δ_b for fixed values of $n_{bo} = 0.5$ and $H = 0.1$.

The reduced equations for $(n, l) = (2, 1)$ are

$$\begin{aligned}
&ik\phi_1^{(2)} - ik\left(\chi + \frac{k^2H^2}{4\chi}\right)N_{e1}^{(2)} \\
&\quad = -\partial_\xi\phi_1^{(1)} + \left(\chi + \frac{k^2H^2}{2\chi}\right)\partial_\xi N_{e1}^{(1)}, \\
&-i\omega N_{i1}^{(2)} + ikV_{i1}^{(2)} = v_g\partial_\xi N_{i1}^{(1)} - \partial_\xi V_{i1}^{(1)}, \\
&-i\omega V_{i1}^{(2)} + ik\phi_1^{(2)} + i\delta_i kN_{i1}^{(2)} = v_g\partial_\xi V_{i1}^{(1)} - \delta_i\partial_\xi N_{i1}^{(1)} - \partial_\xi\phi_1^{(1)}, \\
&-i\omega N_{b1}^{(2)} + ik(1-\chi)V_{b1}^{(2)} = v_g\partial_\xi N_{b1}^{(1)} - (1-\chi)\partial_\xi V_{i1}^{(1)}, \\
&-i\omega V_{b1}^{(2)} + ik\mu\phi_1^{(2)} + i\mu\delta_b k(1-\chi)N_{b1}^{(2)} \\
&\quad = v_g\partial_\xi V_{b1}^{(1)} - \mu\delta_b(1-\chi)\partial_\xi N_{b1}^{(1)} - \mu\partial_\xi\phi_1^{(1)}, \\
&\chi N_{e1}^{(2)} - N_{i1}^{(2)} - (1-\chi)N_{b1}^{(2)} + k^2\phi_1^{(2)} = 2ik\partial_\xi\phi_1^{(1)}.
\end{aligned} \tag{13}$$

The compatibility condition obtained from the above-reduced equations is

$$\begin{aligned}
v_g &= \frac{-1 + \frac{2H^2\chi^2}{(H^2k^2 + 4\chi^2)} + \omega^2\left[\frac{(\chi-1)^2\mu}{(\omega^2 - k^2(\chi-1)^2\mu\delta_b)^2} + \frac{1}{(\omega^2 - k^2\delta_i)^2}\right]}{k\omega\left[\frac{(\chi-1)^2\mu}{(\omega^2 - k^2(\chi-1)^2\mu\delta_b)^2} + \frac{1}{(\omega^2 - k^2\delta_i)^2}\right]} \\
&= \frac{\partial\omega}{\partial k}.
\end{aligned} \tag{14}$$

In Eq. (14), v_g represents the group velocity of the wavepackets. The variation in v_g with k for different values of plasma parameters n_{bo}, H, and δ_b is illustrated in Figure 2. In every case, the group velocity begins large at small k values and decreases as k increases. It is observed from Figure 2(a) that v_g rises with an increase in n_{bo}; however, for large values of k, it reaches zero slowly. Figure 2(b) shows that, for smaller k values, v_g increases with an increase in H; however, after some values of k, the trend changes and v_g decreases with an increase in H. Furthermore, for small k values, v_g is not influenced by δ_b, and for large k values, v_g rises as δ_b increases, as shown in Figure 2(c).

The reduced equations of second-order, $n = 2$, $l = 1$, result in

$$\begin{aligned}
N_{e1}^{(2)} &= \left(\frac{4H^2k^2\chi + 16\chi^3}{(4\chi^2 + k^2H^2)^2}\right)\phi_1^{(2)} + i\left(\frac{4H^2k\chi}{(4\chi^2 + k^2H^2)^2}\right)\partial_\xi\phi_1^{(1)}, \\
N_{i1}^{(2)} &= -\left(\frac{k^4\delta_i - k^2\omega^2}{(\omega^2 - k^2\delta_i)^2}\right)\phi_1^{(2)} - i\left(\frac{2k\omega(\omega - kv_g)}{(\omega^2 - k^2\delta_i)^2}\right)\partial_\xi\phi_1^{(1)}, \\
V_{i1}^{(2)} &= -\left(\frac{k\omega^3 + k^3\omega\delta_i}{(\omega^2 - k^2\delta_i)^2}\right)\phi_1^{(2)} + i\left(-\frac{(\omega^3 + k^2\omega\delta_i)}{(\omega^2 - k^2\delta_i)^2}\right. \\
&\quad \left. + \frac{k\omega^2v_g + k^3V_g\delta_i}{(\omega^2 - k^2\delta_i)^2}\right)\partial_\xi\phi_1^{(1)}, \\
N_{b1}^{(2)} &= \left(\frac{k^2(\chi-1)\mu(-\omega^2 + k^2(\chi-1)^2\mu\delta_b)}{(\omega^2 - k^2\mu\delta_b(\chi-1)^2)^2}\right)\phi_1^{(2)} + iA_{b1}\partial_\xi\phi_1^{(1)}, \\
V_{b1}^{(2)} &= -\mu\left(\frac{-k\omega^3 + k^3(\chi-1)^2\mu\omega\delta_b}{(\omega^2 - k^2\mu\delta_b(\chi-1)^2)^2}\right)\phi_1^{(2)} + iA_{b2}\partial_\xi\phi_1^{(1)}.
\end{aligned} \tag{15}$$

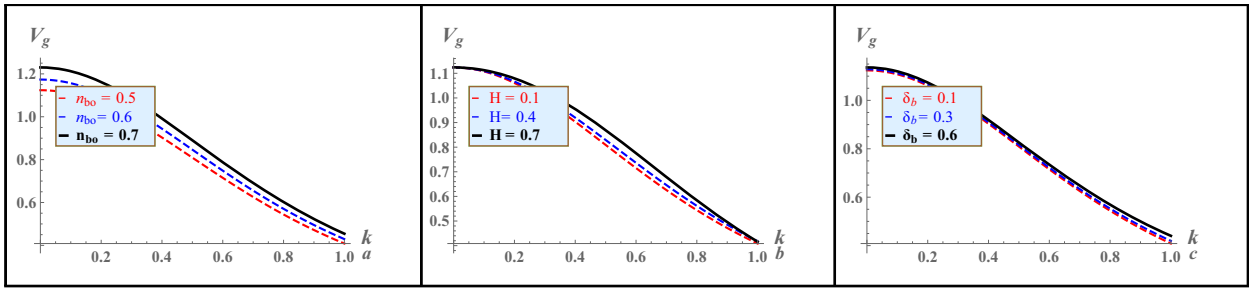

Figure 2: The wave packets group velocity v_g is analyzed against (a) ion beam density n_{bo} for fixed values of $H = 0.1$ and $\delta_b = 0.1$, (b) quantum diffraction parameter H for fixed values of $n_{bo} = 0.5$ and $\delta_b = 0.1$, and (c) ion beam temperature δ_b for fixed values of $n_{bo} = 0.5$ and $H = 0.1$.

The coefficients A_{b1} and A_{b2} are given in the Appendix. The second harmonic quantities obtained from the reduced equations for $(n, l) = (2,2)$ read

$$\begin{aligned} N_{e2}^{(2)} &= (A_3^3 + A_4^4 A_9^9)|\phi_1^{(1)}|^2, \\ N_{i2}^{(2)} &= -(A_5^5 + A_6^6 A_9^9)|\phi_1^{(1)}|^2, \\ V_{i2}^{(2)} &= (A_{10}^{10} + A_{11}^{11} A_9^9)|\phi_1^{(1)}|^2, \\ N_{b2}^{(2)} &= (-A_7^7 + A_8^8 A_9^9)|\phi_1^{(1)}|^2, \\ V_{b2}^{(2)} &= (-A_{12}^{12} + A_{13}^{13} A_9^9)|\phi_1^{(1)}|^2, \\ \phi_2^{(2)} &= A_9^9 \, |\phi_1^{(1)}|^2. \end{aligned} \tag{16}$$

The second-order zero harmonic quantities obtained from reduced equations for $(n, l) = (2, 0)$ are

$$\begin{aligned} N_{e0}^{(2)} &= -\left(\frac{16\chi}{(H^2k^2 + 4\chi^2)^2} - \frac{A_{22}^{22}}{\chi}\right)|\phi_1^{(1)}|^2, \\ N_{i0}^{(2)} &= -(A_{14}^{14} + A_{15}^{15} A_{22}^{22})|\phi_1^{(1)}|^2, \\ V_{i0}^{(2)} &= -(A_{16}^{16} + A_{17}^{17} A_{22}^{22})|\phi_1^{(1)}|^2, \\ N_{b0}^{(2)} &= -(A_{18}^{18} + A_{19}^{19} A_{22}^{22})|\phi_1^{(1)}|^2, \\ V_{b0}^{(2)} &= (A_{20}^{20} + A_{21}^{21} A_{22}^{22})|\phi_1^{(1)}|^2, \\ \phi_0^{(2)} &= A_{22}^{22} \, |\phi_1^{(1)}|^2. \end{aligned} \tag{17}$$

Finally, we obtain the following cubic NLSE by substituting the above derived expressions into the $l = 1$ component of the third-order part of the reduced equations:

$$i\frac{\partial \Psi}{\partial \tau} + P\partial_\xi^2 \Psi + Q\,|\Psi|^2\Psi = 0. \tag{18}$$

Eq. (18) is referred to as NLSE, with $\phi_1^{(1)} = \Psi$, where the group dispersion coefficient P and the nonlinear coefficient Q are given by

$$\begin{aligned} P = &\left[\frac{(-\omega^2 + k^2(\chi-1)^2\mu\delta_b)(\omega^2 - k^2\delta_i)^2}{(\omega^2 - k^2\delta_i)^2((1-\chi)\omega A_1^1 + k(1-\chi)(\chi-1)A_2^2) - (-\omega^2 + k^2(\chi-1)^2\mu\delta_b)(2k^2\omega^3 + 2k^4\omega\delta_i)}\right] \\ &\times \left\{1 - \frac{16(H^4k^2\chi^4 + 4H^2\chi^6)}{(H^2k^2 + 4\chi^2)^4} + \frac{(kv_g - \omega)(\omega^2(\omega - 3kv_g) + k^2(3\omega - kv_g)\delta_i)}{(\omega^2 - k^2\delta_i)^3} \right. \\ &\left. + \frac{(1-\chi)((\chi-1)A_{b2}(\omega - kv_g) + 2A_{b1}(\omega v_g - k(\chi-1)^2\mu\delta_b))}{-\omega^2 + k^2(\chi-1)\mu\delta_b}\right\}, \end{aligned} \tag{19}$$

and

$$\begin{aligned} Q = &\left[\frac{(-\omega^2 + k^2(\chi-1)^2\mu\delta_b)(\omega^2 - k^2\delta_i)^2}{(\omega^2 - k^2\delta_i)^2((1-\chi)\omega A_1^1 + k(1-\chi)(\chi-1)A_2^2) - (-\omega^2 + k^2(\chi-1)^2\mu\delta_b)(2k^2\omega^3 + 2k^4\omega\delta_i)}\right] \\ &\times \left\{-\frac{8\chi^2(-15H^2k^2\chi^4 + 32\chi^2)}{(H^2k^2 + 4\chi^2)^4} - \frac{2(3H^2k^2 - 8\chi^2)(\chi A_3^3 + \chi A_4^4 A_9^9 + A_{22}^{22})}{(H^2k^2 + 4\chi^2)^2} - \frac{k(1-\chi)(\omega A_2^2(A_7^7 - A_8^8 A_9^9))}{-\omega^2 + k^2(\chi-1)^2\mu\delta_b} - \right. \\ &\frac{k(1-\chi)(\omega A_1^1(-A_{12}^{12} + A_9^9 A_{13}^{13} + A_{20}^{20} + A_{21}^{21}A_{22}^{22}) - k(1-\chi)A_2^2(-A_{12}^{12} + A_9^9 A_{13}^{13} + A_{20}^{20} + A_{21}^{21}A_{22}^{22}) + k(\chi-1)\mu A_1^1(A_7^7 - A_8^8 A_9^9)\delta_b)}{-\omega^2 + k^2(\chi-1)^2\mu\delta_b} \\ &- \frac{k^2(-\omega(\omega A_5^5 + \omega A_6^6 A_9^9 + \omega(A_{14}^{14} + A_{15}^{15}A_{22}^{22}) + 2k(-A_{10}^{10} - A_9^9 A_{11}^{11} + A_{16}^{16} + A_{17}^{17}A_{22}^{22})) - k^2(A_5^5 + A_6^6 A_9^9 + A_{14}^{14} + A_{15}^{15}A_{22}^{22})\delta_i)}{(\omega^2 - k^2\delta_i)^2} \\ &\left. - \frac{k(1-\chi)(A_{18}^{18} + A_{19}^{19}A_{22}^{22})(\omega A_2^2 + k(\chi-1)\mu A_1^1\delta_b)}{-\omega^2 + k^2(\chi-1)^2\mu\delta_b}\right\} \end{aligned} \tag{20}$$

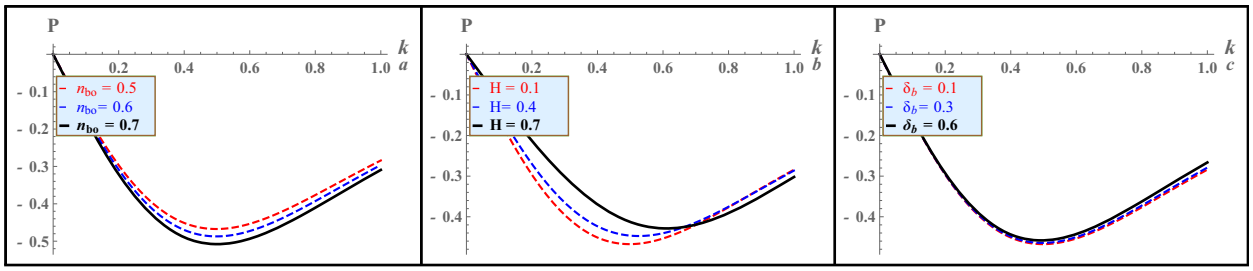

Figure 3: The coefficient P is analyzed against (a) ion beam density n_{bo} for fixed values of $H = 0.1$ and $\delta_b = 0.1$, (b) quantum diffraction parameter H for fixed values of $n_{bo} = 0.5$ and $\delta_b = 0.1$, and (c) ion beam temperature δ_b for fixed values of $n_{bo} = 0.5$ and $H = 0.1$.

The coefficient P related to wave packets group velocity v_g *via* $P = \frac{1}{2}\frac{\partial v_g}{\partial k}$ is examined against k for different values of n_{bo}, H, and δ_b as displayed in Figure 3. It is shown that P is always negative in the given range for all parameters (n_{bo}, H, δ_b). The absolute value of P first rises and reaches its maximum value, then decreases as k increases. It is also observed that a rise in the maximum absolute value of P occurs with an increase in the n_{bo}, as depicted in Figure 3(a). Furthermore, the maximum absolute value of P falls with an increase in H and δ_b, as shown in Figure 3(b) and (c).

The nonlinearity coefficient Q due to carrier wave self-interaction turns negative for larger wave number k, as shown in Figure 4. The modulational stable region corresponds to the positive sign of Q (*i.e.*, $Q > 0$ or $k < k_C$). In contrast, the negative sign of Q indicates a modulational unstable region (*i.e.*, $Q < 0$ or $k_C < k$).

4 MI analysis

We now provide a quick overview of the NLSE (18) stability analysis by linearizing around the monochromatic (Stokes') wave solution [92,93] of the form $\Psi = \psi \exp[iQ|\psi|^2\tau]$, where ψ is set to equal $\psi_o + \varepsilon\psi_1$. The perturbation ψ_1 is represented in this case as $\psi_1 = \psi_{1,0}\exp[i(\hat{k}\xi - \hat{\omega}\tau)] + c.c.$, where $c.c$ for the complex conjugate, $\hat{\omega}$, and $\hat{k}$ denote perturbed frequency and perturbed wave number. It is important to distinguish $\hat{\omega}$ and $\hat{k}$ from k and ω. The following nonlinear dispersion relation is obtained for amplitude modulation by substituting it into Eq. (18):

$$\hat{\omega}^2 = P^2\hat{k}^2\left(\hat{k}^2 - \frac{2Q}{P}|\psi_{1,0}|^2\right). \tag{21}$$

The stability/instability of plane-wave solutions under external perturbations can be inferred from the signs of P and Q [94]. The carrier wave's amplitude is modulationally stable if Q/P is negative, as demonstrated by Eq. (21). In this case, the angular frequency $\hat{\omega}$ remains real for all values of $\hat{k}$, and no instability occurs. However, MI begins when $\hat{\omega}$ becomes imaginary for the positive sign of Q/P. The MI is attained at perturbation wave number $\hat{k} = \hat{k_C} = \sqrt{2\frac{Q}{P}}|\psi|$, where ψ denotes the amplitude of the carrier waves. The expression for the MI growth rate obtained from Eq. (21) is

$$\Gamma = P\hat{k}^2\sqrt{\frac{k_C^2}{\hat{k}^2} - 1} = \mathrm{Im}[\hat{\omega}]. \tag{22}$$

Before we proceed to envelope solitons formation, we should first identify parametric stable and unstable regions based on the sign of Q/P. The sign of Q/P depends

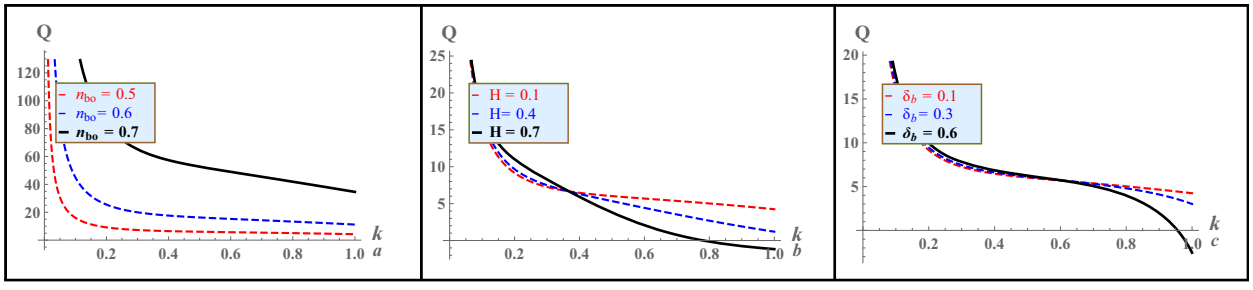

Figure 4: The coefficient Q is analyzed against (a) ion beam density n_{bo} for fixed values of $H = 0.1$ and $\delta_b = 0.1$, (b) quantum diffraction parameter H for fixed values of $n_{bo} = 0.5$ and $\delta_b = 0.1$, and (c) ion beam temperature δ_b for fixed values of $n_{bo} = 0.5$ and $H = 0.1$.

upon the wave number k and plasma parameters (n_{bo}, H, δ_b), as shown in Figure 5. For small wave numbers k (*i.e.*, for larger wavelengths), the ratio Q/P is negative, which suggests modulational stability of the wave packets as expected physically. However, the ratio Q/P becomes positive for the wave numbers greater than certain critical wave number k_C (where $Q = 0$ or $Q/P = 0$), indicating that MI begins above k_C. For $n_{bo} = 0.5$, the value of k_C is approximately 1.5, and it approaches greater values as n_{bo} increases, as displayed in Figure 5(a). This depicts that the modulationally unstable region (or growth rate) grows with higher values of n_{bo}. The value of k_C is approximately 1.42 for $H = 0.1$ and reduces as H increases. This shows that the modulationally unstable region diminishes with rising values of H. Our findings are consistent with those of Mishra and Ghosh [95]. The quantitative impact of H and δ_b on the k_C is quite comparable. The impact of diverse plasma parameters (n_{bo}, H, δ_b) on the ratio Q/P is shown in Figure 5. We noted from Figure 5(a) that the absolute value of the ratio Q/P both in the modulationally stable ($k < k_C$) and unstable ($k_c < k$) regions increases with rising values of n_{bo}, suggesting the formation of narrower black and bright envelope solitons. The impact of the diffraction parameter H on the ratio Q/P as a function of k (keeping n_{bo} and δ_b constant) is illustrated in Figure 5(b). It is demonstrated that in modulationally stable (*i.e.*, $k < k_C$) and unstable (*i.e.*, $k_C < k$) regions, the absolute value of Q/P increases with higher H values for a given value of k. An analogous quantitative pattern for increasing values of δ_b is also seen in Figure 5(c).

5 Envelope soliton formation

In this study, we examined IAWs in quantum plasma with an ion beam. Model quantum plasma is considered for the numerical analysis by choosing the values for ion beam density n_{bo} and ion beam temperature δ_b based on the work of Indrani Paul *et al.* [83], and quantum diffraction parameter H values from Hass *et al.* [14], which corresponds to the laser-produced quantum plasmas.

The nonlinear excitations in the form of bright and dark envelope solitons are described by the localized solution of the NLSE (18). By using $\Psi(\tau, \xi) = (\rho)^{\frac{1}{2}} \exp[i\Theta]$. in Eq. (18) and equating real and imaginary parts, the exact expressions for these envelope structures can be determined. For a detailed derivation, the reader is advised to see previous studies [64,93].

The bright soliton solution of NLSE (18) is associated with a positive sign of Q/P. In the region of larger wave numbers or shorter wavelengths, the carrier wave is modulationally unstable, and it can either grow to bright-type solitons or collapse as a result of random external perturbations. Bright solitons solution represents localized envelope pulses that restrict the fast carrier wave. The exact expressions for bright-type solitons. [93] are given by

$$\begin{cases} \Psi = \sqrt{\Psi_m}\, \mathrm{sech}\left(\dfrac{\xi - V\tau}{L}\right), \\ \Theta = \dfrac{1}{2P}[V\xi - (V^2/2 + \Lambda)\tau], \end{cases} \tag{23}$$

where V, L, and Λ denote the envelope velocity, pulse width, and oscillation frequency at rest. It is observed that, in contrast to the KdV equation where $L^2\Psi_m = \mathrm{cons\,tan}t$, Ψ_m and L satisfy $L\Psi_m = \sqrt{2P/Q} = \mathrm{cons\,tan}t$ (available in complete detail in the study of Kourakis and Shukla [64]). The pulse amplitude is independent of V, and the phase profile of the bright envelope solitons remains the same during their propagation. The slight deformation in the internal structure of the envelope is due to the slow dependency of its phase on space and time. The bright envelope soliton solution (23) is numerically examined against the relevant plasma parameters (n_{bo}, H, δ_b), as shown in Figure 6. We noted that relevant plasma parameters influence the structure of bright solitons. The amplitude and phase of the bright solitons are shifted with relevant plasma parameters (n_{bo}, H, δ_b).

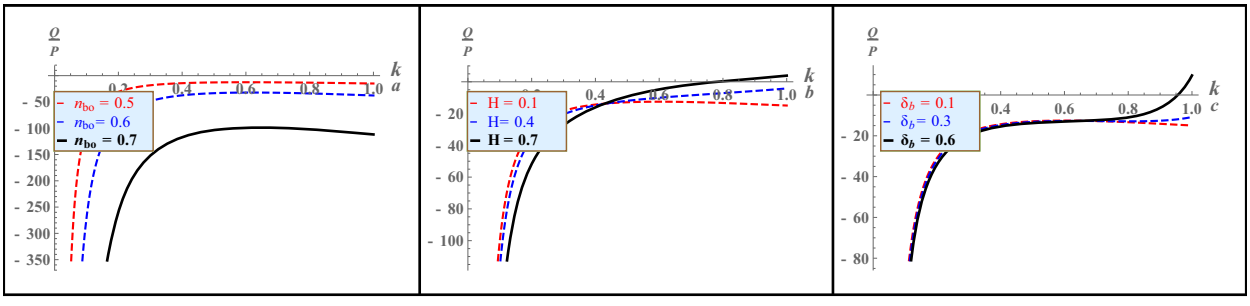

Figure 5: The ratio Q/P is analyzed against (a) ion beam density n_{bo} for fixed values of $H = 0.1$ and $\delta_b = 0.1$, (b) quantum diffraction parameter H for fixed values of $n_{bo} = 0.5$ and $\delta_b = 0.1$, and (c) ion beam temperature δ_b for fixed values of $n_{bo} = 0.5$ and $H = 0.1$.

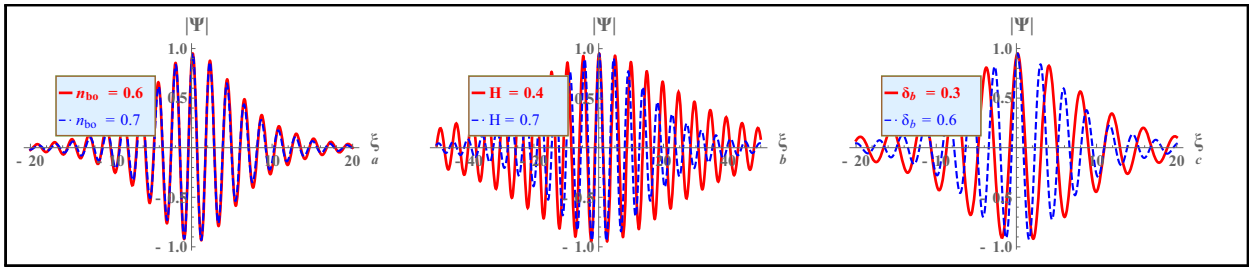

Figure 6: Bright envelope soliton solution (23) is plotted in unstable region (*i.e.*, $Q/P > 0$) against (a) ion beam density n_{bo} for fixed values of $H = 0.1$ and $\delta_b = 0.1$, (b) quantum diffraction parameter H for fixed values of $n_{bo} = 0.5$ and $\delta_b = 0.1$, and (c) ion beam temperature δ_b for fixed values of $n_{bo} = 0.5$ and $H = 0.1$.

Dark envelope soliton solution of NLSE (18) is associated with a negative sign of Q/P. In the region represented by small k values or longer wavelenghts, the carrier wave is modulationally stable and it may take the form of dark-type solitons, which are propagating localized envelope holes (voids). The exact expressions for dark solitons [93] are given by

$$\begin{cases} \Psi = \Psi_m\left(1 - d^2\,\mathrm{sech}^2\left(\dfrac{\xi - u\tau}{L_1}\right)\right), \\ \Theta = \dfrac{1}{2P}(u_0\xi - (\dfrac{1}{2}u_o^2 - 2PQ\Psi_m)\tau). \end{cases} \tag{24}$$

These excitations can appear as black solitons (vanishing potential at $\xi = 0$) or gray solitons (finite potential at $\xi = 0$), the asymptotic values in both cases at infinite are constant and finite. The value of constant d is equal to one for black solitons and less than one for gray solitons. The numerical examination of the dark-type envelope soliton solution (24) against plasma parameters (n_{bo}, H, δ_b) is displayed in Figures 7 and 8. These figures show that plasma parameters (n_{bo}, H, δ_b) influence the structure of both dark and gray envelope solitons that slowly shift the amplitude and phase of the modulated dark solitons.

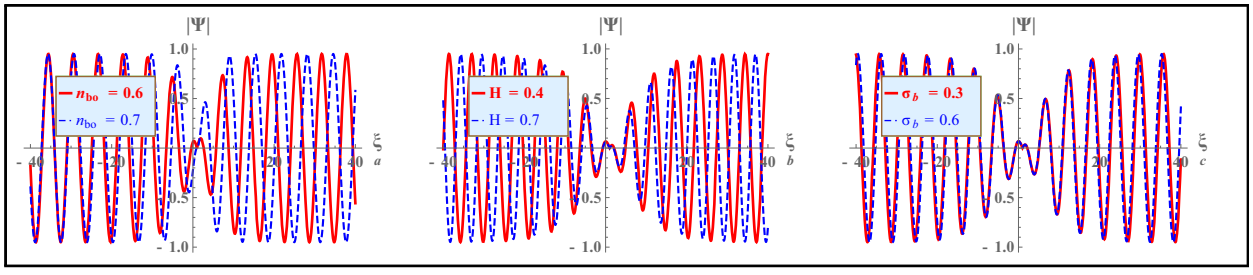

Figure 7: Dark (black) envelope soliton solution (24) is plotted in stable region (*i.e.*, $Q/P < 0$ and $d = 1$) against (a) ion beam density n_{bo} for fixed values of $H = 0.1$ and $\delta_b = 0.1$, (b) quantum diffraction parameter H for fixed values of $n_{bo} = 0.5$ and $\delta_b = 0.1$, and (c) ion beam temperature δ_b for fixed values of $n_{bo} = 0.5$ and $H = 0.1$.

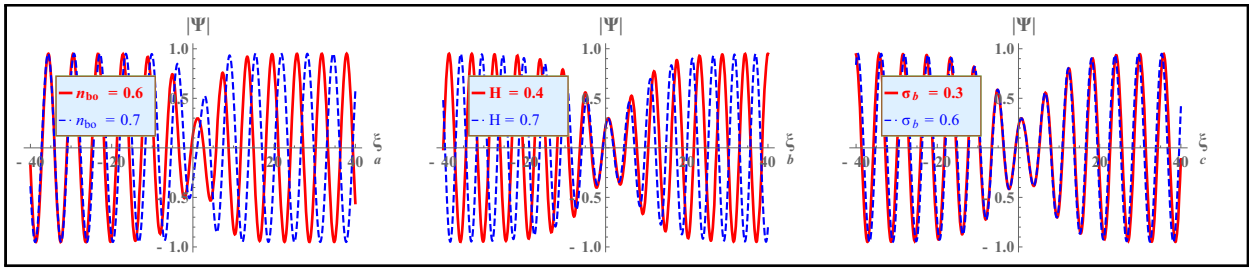

Figure 8: Dark (gray) envelope soliton solution (24) is plotted in stable region (*i.e.*, $Q/P < 0$ and $d = 0.95$) against (a) n_{bo} while keeping $H = 0.1$ and $\delta_b = 0.1$, (b) H whiel keeping $n_{bo} = 0.5$ and $\delta_b = 0.1$, and (c) δ_b whiel keeping $n_{bo} = 0.5$ and $H = 0.1$.

6 Summary

In this article, we have studied the low-frequency IAWs in unmagnetized quantum plasma including the effects of ion beams. One of the reductive perturbation methods, *i.e.*, DEM has been used for reducing the basic plasma model equations to the cubic NLSE. The nonlinearity and dispersion coefficients of the NLSE have been explicitly expressed, and their parametric dependency on the relevant plasma parameters has been investigated. The MI and growth rate of envelope excitations have been estimated based on the coefficients of the NLSE. We noted that the critical wavenumber k_C grows as the ion beam density n_{bo} values increase. Conversely, k_C decreases when the quantum parameter H and the ion beam temperature ratio δ_b increase, suggesting that MI occurs at lower k. It was shown that the instability growth rate decreases when H and δ_b values increase. However, it was found that increasing the values of n_{bo} results in an increase in the instability growth rate. Furthermore, the rising values of all relevant plasma parameters (n_{bo}, H, δ_b) lead to narrower dark and bright solitons in modulationally stable and unstable regions.

For clarity and precision, it is important to highlight that we have utilized a QHD model, which incorporates two key quantum effects, *i.e.*, Bohm potential and and quantum statistical terms. Our model is valid for small values of H. The existence of quantum plasma has been confirmed in astrophysical environments, (viz., neutron stars, white dwarfs, and supernovae remnants) and in laser-driven plasma compression experiments [5]. The number densities in these systems can reach values as high as 10^{23} and 10^{32} m^{-3} at $T_{\mathrm{Fe}} = 10^5$ K, resulting in numerical values of $H \sim 1$ and 10^{-2}. For technological and laboratory plasmas, the values of H are typically less than one, while they exceed unity for superdense astrophysical plasmas [96]. One of the most significant anticipated applications of this study is the utilization of quantum plasma for the self-cooling of quantum computer components. This entails regulating the instability regions by manipulating plasma parameters that influence their thickness, potentially mitigating the enigmatic phenomena that can raise the temperatures of electronic chips. The study may also be beneficial for analyzing nonlinear effects in sensing signals, signal propagation in optical communications, and the design of optical fibers [97]. Furthermore, our findings may contribute to a better understanding of beam–plasma interactions and the dynamics of nonlinear structures within dense quantum plasmas.

7 Future work

The phenomena of RWs and breathers are among the most enigmatic occurrences, producing many consequences that can significantly influence the features of the system under investigation. Consequently, future research may investigate the characteristics of nonplanar RWs and breathers [98–101], dissipative RWs and breathers [102,103], as well as the methods for regulating their manifestation in the system under examination, depending on the necessity for their presence or avoidance.

Acknowledgments: The authors aknowledge the financial support provided by Princess Nourah bint Abdulrahman University Researchers Supporting Project number (PNURSP2025R439), Princess Nourah bint Abdulrahman University, Riyadh, Saudi Arabia. The support of Prince sattam bin Abdulaziz University project number (PSAU/2025/R/1446) is also acknowledged.

Funding information: The authors are thankful for the financial support provided by Princess Nourah bint Abdulrahman University Researchers Supporting Project number (PNURSP2025R439), Princess Nourah bint Abdulrahman University, Riyadh, Saudi Arabia. The support of Prince sattam bin Abdulaziz University project number (PSAU/2025/R/1446) is also acknowledged.

Author contributions: Fazal Wahed: formal analysis, investigation, writing – original draft. Ata-ur-Rahman: methodology, writing – review and editing. S. Neelam Naeem: investigation, writing – original draft. R. A. Alharbey: investigation, methodology. Maryam Al Huwayz: formal analysis, writing – original draft. Lamiaa S. El-Sherif: investigation, writing – review and editing. Samir A. El-Tantawy: formal analysis, investigation, methodology, supervision, writing – review and editing. All authors have accepted responsibility for the entire content of this manuscript and approved its submission.

Conflict of interest: The authors state no conflict of interest.

Data availability statement: All data generated or analysed during this study are included in this published article.

References

[1] Killian TC. Ultracold neutral plasmas. Sci. 2007;316:705–8.
[2] Marklund M, Shukla PK. Nonlinear collective effects in photon-photon and photon-plasma interactions. Rev M Phy. 2006;78:591.

[3] Becker K, Koutsospyros A, Yin SM, Christodoulatos C, Abramzon N, Joaquin JC, et al. Environmental and biological applications of microplasmas. Plasma Phys Contrl Fus. 2005;47:513.
[4] Markowich PA, Ringhofer CA, Schmeiser C. The drift diffusion equations. Semiconductor equations. New York: Springer-Verlag; 1990. p. 104–74.
[5] Jung YD. Quantum-mechanical effects on electron-electron scattering in dense high-temperature plasmas. Phys Plasmas. 2001;8(8):3842–4.
[6] Hossen MA, Hossen MR, Mamun AA. Modified ion-acoustic shock waves and double layers in a degenerate electron-positron-ion plasma in presence of heavy negative ions. Braz J Phys. 2014;44:703–10.
[7] Manfredi G. Proceedings of the Workshop on kinetic theory. Fields Inst Commun. 2005;46:263.
[8] Qamar A, Rahman A, Mirza AM. Tripolar vortex formation in dense quantum plasma with ion-temperature gradients. Phys Plasmas. 2012;19:052303.
[9] Hass F. Quantum plasmas. An hydrodynamic approach. New York, NY, USA: Springer; 2011.
[10] Madelung E. Quantum theory in hydrodynamic form. Z Phys. 1927;40:322–36.
[11] Manfredi G, Haas F. Self-consistent fluid model for a quantum electron gas. Phys Rev B. 2001;64:075316.
[12] Gardner CL. The quantum hydrodynamic model for semiconductor devices. SIAM J Appl Maths. 1994;54:409–27.
[13] Gardner CL. Numerical simulation of a steady-state electron shock wave in a submicrometer semiconductor device. IEEE Trans Electron Devices. 1991;38:392–8.
[14] Haas H, Garcia LG, Goedert J. Quantum ion-acoustic waves. Phys Plasmas. 2003;10:3858.
[15] Mushtaq A, Khan SA. Ion acoustic solitary wave with weakly transverse perturbations in quantum electron-positron-ion plasma. Phys Plasmas. 2007;14:052307.
[16] Rajabi B, Mohammadnejad M. Modulational instability of ion-acoustic waves in a dense quantum plasma. Phys Plasmas. 2023;8:30.
[17] Chandra S, Paul SN, Ghosh B. Linear and non-linear propagation of electron plasma waves in quantum plasma. Indian J Pure Appl Phys. 2012;50:314–9.
[18] Celata CM, Bieniosek FM, Henestroza E, Kwan JW, Lee EP, Logan G, et al. Progress in heavy ion fusion research. Phys Plasmas. 2003;10:2064–70.
[19] Sharp WM, Callahan DA, Tabak M, Yu SS, Peterson PF, Welch DR, et al. Modeling chamber transport for heavy-ion fusion. Fusion Sci Tech. 2003;43:393–400.
[20] Davidson RC, Logan BG, Barnard JJ, Bieniosek FM, Briggs RJ, Callahan DA, et al. US heavy ion beam research for high energy density physics applications and fusion. In J de Phys IV (Proceedings) EDP Sci. 2006;133:731–41.
[21] Colak S, Fitzpatrick BJ, Bhargava RN. Electron beam pumped II–VI lasers. J Cryst Growth. 1985;72:504.
[22] Gurskii AL, Lutsenko EV, Mitcovets AI, Yablonskii GP. High-efficiency electron-beam-pumped semiconductor laser emitters. Phys B. 1993;185:505.
[23] Liu L, Jia L, Liang Z, Sankai S, Xifeng R. Polarization independent tunable near-perfect absorber based on graphene-BaO arrays and Ag-dielectric Bragg reflector composite structure. Diamond Relat Mater. 2025;152:111958.
[24] Richa, Bhupendra KS, Bandar A, David L. Intelligent neuro-computational modelling for MHD nanofluid flow through a curved stretching sheet with entropy optimization: Koo–Kleinstreuer–Li approach. J Comput Des Eng. 2024;11:164–83.
[25] Sorensen AH, Bonderup E. Electron cooling. Nucl Instrum Methods Phys Res. 1983;215:27.
[26] Goldman SR, Hofmann I. Electron cooling of high-Z ion beams parallel to a guide magnetic field. IEEE Trans Plasma Sci. 1990;18:789.
[27] Kumar A, Sharma BK, Almohsen B, Pérez LM, Urbanowicz K. Artificial neural network analysis of Jeffrey hybrid nanofluid with gyrotactic microorganisms for optimizing solar thermal collector efficiency. Sci Rep. 2025;15(1):4729.
[28] Shilei X, Nan Y, Haoyu G, Guangyuan S, Ming L, Yoshihiro D, et al. Combination of plasma acoustic emission signal and laser-induced breakdown spectroscopy for accurate classification of steel. Anal Chim Acta. 2025;1336:343496.
[29] Anup K, Bhupendra KS, Madhu S, Bandar A, Ioannis ES. Entropy generation optimization for casson hybrid nanofluid flow along a curved surface with bioconvection mechanism and exothermic/endothermic catalytic reaction. Adv Theor Simul. 2025;8:2401554.
[30] Krushelnick K, Clark EL, Allott R, Beg FN, Danson CN, Machacek A, et al. Ultrahigh-intensity laser-produced plasmas as a compact heavy ion injection source. IEEE Trans Plasma Sci. 2000;28:1184.
[31] Kaganovich ID, Startsev EA, Sefkow AB, Davidson RC. Charge and current neutralization of an ion-beam pulse propagating in a background plasma along a solenoidal magnetic field. Phys Rev Lett. 2007;99:235002.
[32] Renk TJ, Mann GA, Torres GA. Performance of a pulsed ion beam with a renewable cryogenically cooled ion source. Laser Particle Beams. 2008;26:545.
[33] Goldman MV. Progress and problems in the theory of type III solar radio emission. Solar Phys. 1983;89:403–42.
[34] Hoffmann RA, Evans DS. Field-aligned electron bursts at high latitudes observed by Ogo 4. J Geophys Res. 1968;73:6201–14.
[35] Alotaibi MA, El-Sapa S. Effect of permeability on the interaction between two spheres translating through a couple stress fluid. Fluid Dyn Res. 2025; 57(1):015503.
[36] Al-Hanaya A, El-Sapa S. Impact of permeability and fluid parameters in couple stress media on rotating eccentric spheres. Open Phys. 2024;22(1):20240112.
[37] El-Sapa S, Alotaibi MA. Migration of two rigid spheres translating within an infinite couple stress fluid under the impact of magnetic field. Open Phys. 2024;22(1):20240085.
[38] Krivoruchko SM, Fainberg VB, Shapiro VD, Shevchenko VI. Solitary charge density waves in a magnetoactive plasma. Sov JETP. 1975;40:1039–43.
[39] Deka MK, Adhikary NC, Misra AP, Bailung H, Nakamura Y. Characteristics of ion-acoustic solitary wave in a laboratory dusty plasma under the influence of ion-beam. Phys Plasmas. 2012;19:103704.
[40] Chatterjee P, Roychoudhury R. The effect of finite ion temperature on solitary waves in a plasma with an ion beam. Phys Plasmas. 1995;2:1352.
[41] Abrol PS, Tagare SG. Ion-acoustic solitary waves in an ion-beam–plasma system with nonisothermal electrons. Phys Lett A. 1979;75:74–6.
[42] Gell Y, Roth I. The effects of an ion beam on the motion of solitons in an ion beam–plasma system. Plasma Phys. 1977;19:915.

[43] Das R, Deka P. Korteweg-de Vries solutions in high relativistic electron beam plasma. Int J Eng Res. 2015;6:864–70.
[44] Misra AP, Adhikary NC. Large amplitude solitary waves in ion-beam plasmas with charged dust impurities. Phys Plasmas. 2011;18:122112.
[45] Huibin L, Kelin W. Solitons in an ion-beam plasma. J Plasma Phys. 1990;44(1):151–65.
[46] Zank GP, McKenzie JF. Solitons in an ion-beam plasma. J Plasma Phys. 1998;39:183–91.
[47] Karmakar B, Das GC, Singh I. Ion-acoustic solitary waves in ion-beam plasma with multiple-electron-temperatures. Plasma Phys Contr Fus. 1988;30:1167.
[48] Kaur N, Singh K, Saini NS. Effect of ion beam on the characteristics of ion acoustic Gardner solitons and double layers in a multicomponent superthermal plasma. Phys Plasmas. 2017;24:092108.
[49] Kaur N, Singh K, Ghai Y, Saini NS. Dust acoustic shock waves in magnetized dusty plasma. Plasma Sci Tech. 2018;20:074009.
[50] Kourakis I, Shukla PK. Oblique amplitude modulation of dust-acoustic plasma waves. Phys Scr. 2004;69:316.
[51] Taniuti T, N. Yajima N. Perturbation method for a nonlinear wave modulation III. J Math Phys. 1969;10:1369.
[52] Albalawi W, El-Tantawy SA, Salas AH. On the rogue wave solution in the framework of a Korteweg-de Vries equation. Results Phys. 2021;30:104847.
[53] Hashmi T, Jahangir R, Masood W, Alotaibi BM, Ismaeel SME, El-Tantawy SA. Head-on collision of ion-acoustic (modified) Korteweg-de Vries solitons in Saturn's magnetosphere plasmas with two temperature superthermal electrons. Phys Fluids. 2023;35:103104.
[54] El-Tantawy SA. Nonlinear dynamics of soliton collisions in electronegative plasmas: The phase shifts of the planar KdV-and mkdV-soliton collisions. Chaos Solitons Fractals. 2016;93:162.
[55] Wazwaz A-M, Alhejaili W, El-Tantawy SA, Study on extensions of (modified) Korteweg-de Vries equations: Painlevé integrability and multiple soliton solutions in fluid mediums. Physics of Fluids. 2023;35:093110.
[56] Kashkari BS, El-Tantawy SA, Salas AH, El-Sherif LS. Homotopy perturbation method for studying dissipative nonplanar solitons in an electronegative complex plasma. Chaos Solitons Fractals. 2020;130:109457.
[57] El-Tantawy SA, Wazwaz A-M. Anatomy of modified Korteweg-de Vries equation for studying the modulated envelope structures in non-Maxwellian dusty plasmas: Freak waves and dark soliton collisions. Phys Plasmas. 2018;25:092105.
[58] Albalawi W, El-Tantawy SA, SAlkhateebadah SA. The phase shift analysis of the colliding dissipative KdV solitons. J Ocean Eng Sci. 2022;7:521.
[59] Gill TS, Bains AS, Saini NS, Bedi C. Ion-acoustic envelope excitations in electron-positron-ion plasma with nonthermal electrons. Phys Lett A. 2010;374:3210–5.
[60] El-Tantawy SA, Wazwaz A-M, Schlickeiser R. Solitons collision and freak waves in a plasma with Cairns-Tsallis particle distributions, Plasma Phys Control Fusion. 2015;57:125012.
[61] Ali Shan S, El-Tantawy SA. The impact of positrons beam on the propagation of super freak waves in electron-positron-ion plasmas. Phys Plasmas. 2016;23:072112.
[62] Esfandyari-Kalejahi A, Kourakis I, Dasmalchi B, Sayarizadeh M. Nonlinear propagation of modulated ion-acoustic plasma waves in the presence of an electron beam. Phys Plasmas. 2006;13:4.
[63] Kourakis I, Shukla PK. Ion-acoustic waves in a two-electron-temperature plasma: oblique modulation and envelope excitations. J Phys A Math Gen. 2003;36:11901.
[64] Kourakis I, Shukla PK. Exact theory for localized envelope modulated electrostatic wavepackets in space and dusty plasmas. Non Pro Geophys. 2005;12:407.
[65] Esfandyari-Kalejahi A, Asgari H. Ion-acoustic solitary excitations in a two-electron-temperature plasma with adiabatic warm ions. Phys Plasmas. 2005;12:102302.
[66] Krall NA, Trivelpiece AW. Fundamentals of plasma physics and principles of plasma physics. NewYork: McGraw-Hill; 1973.
[67] Stix T. Waves in plasmas. New York: American Institute of Physics; 1992.
[68] Rahman A. Electrostatic Rogue waves in a degenerate Thomas-Fermi plasma. Braz J Phys. 2019;49:517–25.
[69] Irshad M, Khalid M. Modulational instability of ion acoustic excitations in a plasma with a kappa-deformed Kaniadakis electron distribution. Eur Phys J Plus. 2022;137:893.
[70] Kivshar Yu S, Peyrard M. Modulational instabilities in discrete lattices. Phys Rev A. 1992;46:3198.
[71] Remoissenet M. Waves called solitons. Berlin: Springer; 1994.
[72] Hasegawa A. Plasma instabilities and nonlinear effects. Berlin: Springer; 1975.
[73] Shukla PK, Stenflo L, Fedele R. Modulational instability of two colliding Bose–Einstein condensates. Phys Scr. 2001;64:553.
[74] Theocharis G, Rapti Z, Kevrekidis PG, Frantzeskakis DJ, Konotop VV. Modulational instability of Gross-Pitaevskii-type equations in 1 + 1 dimensions. Phys Rev A. 2003; 67:063610.
[75] Davydov AS. Solitons in molecular systems. Dordrecht: Kluwer; 1985.
[76] Bilbault JM, Marquie P, Michaux B. Modulational instability of two counterpropagating waves in an experimental transmission line. Phys Rev E. 1995;51:817.
[77] Agrawal G. Fiber optic communication systems. New York: Wiley; 2002.
[78] Watanabe S. Self-modulation of a nonlinear ionwave packet. J Plasma Phys. 1977;17:487.
[79] Irshad M, Khalid M, Khan S, Alotaibi BM, El-Sherif LS, El-Tantawy SA. Effect of kappa-deformed Kaniadakis distribution on the modulational instability of electron-acoustic waves in a non-Maxwellian plasma. Phys Fluids. 2023:35:105116.
[80] Wahed F, Rahman AU, Alyousef HA, El-Sherif LS, El-Tantawy SA. Modulational instability and associated low-frequency dust-acoustic waves in a degenerate Thomas-Fermiplasma: Envelope solitons and rogue waves. J Low Freq Noise Vibr Act Control. 2024;16:14613484241308433.
[81] El-Tantawy SA. Ion-acoustic waves in ultracold neutral plasmas: modulational instability and dissipative rogue waves. Phys Lett. 2017;381:787–91.
[82] Kourakis I, Shukla PK. Electron-acoustic plasma waves: oblique modulation and envelope solitons. Phy Rew E. 2004;69(3):036411.
[83] Paul I, Chatterjee A, Paul SN. Nonlinear propagation of ion acoustic waves in quantum plasma in the presence of an ion beam. Laser Part Beams. 2019;37:370–80.
[84] Az-Zo'bi Emad A. On the reduced differential transform method and its application to the generalized Burgers-Huxley equation. App Math Sci. 2014;8(177):8823–31.
[85] Az-Zo'bi Emad A. Peakon and solitary wave solutions for the modified Fornberg-Whitham equation using simplest equation method. Int J Math Comput Sci. 2019;14(3):635–45.

[86] Asano N, Taniuti T, Yajima N. Perturbation method for a nonlinear wave modulation. II. J Math Phys. 1969;10:2020.
[87] Hasegawa A. Stimulated modulational instabilities of plasma waves. Phys Rev A. 1970;1:1746.
[88] Hasegawa A. Theory and computer experiment on self-trapping instability of plasma cyclotron waves. Phys Fluids. 1972;15(5):870–81.
[89] Debnath L. Nonlinear partial differential equations for scientists and engineers. Birkauser Boston; 2005.
[90] Taniuti T. Reductive perturbation method and far fields of wave equations. Supp Prog Theor Phys. 1974;55:1.
[91] Gardner CS, Morikawa GK. The effect of temperature on the width of a small-amplitude, solitary wave in a collision-free plasma. Comm Pur App Math XVIII. 1965;18:35–49.
[92] Remoissenet R. Waves called solitons. Berlin: Springer; 1996.
[93] Fedele R, Schamel H. Solitary waves in the Madelung's fluid: Connection between the nonlinear Schrödinger equation and the Korteweg-de Vries equation. Eur Phys J B. 2002;27:313.
[94] Dauxois T, Peyrard M. Physics of solitons. Cambridge: Cambridge University Press; 2006.
[95] Misra AP, Ghosh NK. Modulational instability of ion-acoustic wave packets in quantum pair-ion plasmas. Astrophys Space Sci. 2011;331:605–9.
[96] Garcia LG, Haas F, De Oliveira LPL, Goedert J. Modified Zakharov equations for plasmas with a quantum correction. Phys Plasmas. 2005;12(1):012302.
[97] Yu Z, Lü X. Data-driven solutions and parameter discovery of the extended higher-order nonlinear Schrödinger equation in optical fibers. Phys D. 2024;468:134284.
[98] El-Tantawy SA, Aboelenen T. Simulation study of planar and nonplanar super rogue waves in an electronegative plasma: Local discontinuous Galerkin method. Phys Plasmas. 2017;24:052118.
[99] El-Tantawy SA, AlharbeyRA, Salas AH. Novel approximate analytical and numerical cylindrical rogue wave and breathers solutions: An application to electronegative plasma. Chaos Solitons Fractals. 2022;155:111776.
[100] El-Tantawy SA, Salas AH, Alyousef HA, Alharthi MR. Novel approximations to a nonplanar nonlinear Schrödinger equation and modeling nonplanar rogue waves/breathers in a complexplasma. Chaos Solitons Fractals. 2022;1635:112612.
[101] El-Tantawy SA, El-Awady EI. Cylindrical and spherical Akhmediev breather and freak waves in ultracold neutral plasmas. Phys Plasmas. 2018;25:012121.
[102] Aljahdaly NH, El-Tantawy SA, Wazwaz A-M, Ashi HA. Adomian decomposition method for modelling the dissipative higher-order rogue waves in a superthermal collisional plasma. J Taibah Univ Sci. 2021;15:971.
[103] El-Tantawy SA, Salas AH, Alharthi MR. On the analytical and numerical solutions of the linear damped NLSE for modeling dissipative freak waves and breathers in nonlinear and dispersive mediums: an application to a pair-ion plasma. Front Phys. 2021;9:580224.

Appendix

The expressions for the coefficients of Eqs (15), (16), and (17) are:

$$A_{b1} = \frac{2k\mu\omega(\chi-1)(\omega - kv_g)}{(\omega^2 - k^2\mu\delta_b(\chi-1)^2)^2},$$

$$A_{b2} = \frac{\mu(-\omega^3 - k^2(\chi-1))^2\mu\omega\delta_b + kv_g(\omega^2 + k^2(\chi-1)^2\mu\delta_b)}{(\omega^2 - k^2\mu\delta_b(\chi-1)^2)},$$

$$A_1^1 = \frac{k^2(1-\chi)\mu}{\omega^2 - k^2(1-\chi)^2\mu\delta_b},$$

$$A_2^2 = \frac{k\mu\omega}{-\omega^2 + k^2\mu\delta_b - 2k^2\chi\mu\delta_b + k^2\chi^2\mu\delta_b},$$

$$A_3^3 = \frac{\chi(6H^2k^3 - 8k\chi^2)}{k(H^2k^2+\chi^2)(H^2k^2+4\chi^2)^2},$$

$$A_4^4 = \frac{\chi(H^4k^5 + 8H^2k^3\chi^2 + 16k\chi^4)}{k(H^2k^2+\chi^2)(H^2k^2+4\chi^2)^2},$$

$$A_5^5 = \frac{-3k^4\omega^2 - k^6\delta_i}{2(\omega^2 - k^2\delta_i)^3},$$

$$A_6^6 = \frac{-2k^2\omega^4 + 4k^4\omega^2\delta_i - 2k^6\delta_i^2}{2(\omega^2 - k^2\delta_i)^3},$$

$$A_7^7 = \frac{2k\omega A_1^1A_2^2 - k^2(1-\chi)(A_2^2)^2 - k^2(1-\chi)\mu(A_1^1)^2\delta_b}{2\omega^2 - 2k^2(1-\chi)\mu\delta_b},$$

$$A_8^8 = \frac{k^2(1-\chi)\mu}{\omega^2 - k^2(1-\chi)^2\mu\delta_b},$$

$$A_9^9 = \frac{-\chi A_3^3 - A_5^5 - A_7^7 + \chi A_7^7}{4k^2 + \chi A_4^4 + A_6^6 - A_8^8 + \chi A_8^8},$$

$$A_{10}^{10} = \frac{\omega(k^3\omega^2 + 3k^5\delta_i)}{2(\omega^2 - k^2\delta_i)^3},$$

$$A_{11}^{11} = \frac{\omega(2k\omega^4 - 4k^3\omega^2\delta_i + 2k^5\delta_i^2)}{2(\omega^2 - k^2\delta},$$

$$A_{12}^{12} = \frac{-k\omega(A_2^2)^2 - k\mu\omega(A_1^1)^2\delta_b + 2k^2\mu A_1^1A_2^2\delta_b - 2k^2\chi\mu A_1^1A_2^2\delta_b}{2(\omega^2 - k^2\mu\delta_b + 2k^2\chi\mu\delta_b - k^2\chi^2\mu\delta_b)},$$

$$A_{13}^{13} = \frac{k\mu\omega}{\omega^2 - k^2\mu\delta_b + 2k^2\chi\mu\delta_b - k^2\chi^2\mu\delta_b}$$

$$A_{14}^{14} = \frac{-k^2\omega^2 - 2k^3\omega v_g - k^4\delta_i}{(v_g^2 - \delta_i)(k^2\delta_i - \omega^2)^2},$$

$$A_{15}^{15} = \frac{-\omega^4 + 2k^2\omega^2\delta_i - k^4\delta_i^2}{(v_g^2 - \delta_i)(k^2\delta_i - \omega^2)^2},$$

$$A_{16}^{16} = \frac{k^2\omega^2v_g + 2k^3\omega\delta_i + k^4v_g\delta_i}{(\delta_i - v_g^2)(\omega^2 - k^2\delta_i)^2},$$

$$A_{17}^{17} = \frac{\omega^4v_g - 2k^2\omega^2v_g\delta_i + k^4v_g\delta_i^2}{(\delta_i - v_g^2)(\omega^2 - k^2\delta_i)^2},$$

$$A_{18}^{18} = \frac{\mu(\chi-1)(k^2\mu\omega^2 + k^3\mu(2\omega v_g + k(\chi-1)^2\mu\delta_b)}{(v_g^2 - (\chi-1)^2\mu\delta_b)(\omega^2 - k^2(\chi-1)^2\mu\delta_b)^2},$$

$$A_{19}^{19} = \frac{\mu(\chi-1)}{v_g^2 - (\chi-1)^2\mu\delta_b},$$

$$A_{20}^{20} = \frac{\mu(2k^3(\chi-1)^2\mu^2\omega\delta_b + k^2\mu v_g(\omega^2 + k^2(\chi-1)^2\mu\delta_b)}{(v_g^2 - (\chi-1)^2\mu\delta_b)(\omega^2 - k^2(\chi-1)^2\mu\delta_b)^2},$$

$$A_{21}^{21} = \frac{\mu v_g}{v_g^2 - (\chi-1)^2\mu\delta_b},$$

$$A_{22}^{22} = \frac{\frac{16\chi^2}{(H^2k^2+4\chi^2)^2} - A_{14}^{14} + (\chi-1)A_{18}^{18}}{1 + A_{15}^{15} - (\chi-1)A_{19}^{19}}.$$